Biogeosciences, 12, 7453–7465, 2015
www.biogeosciences.net/12/7453/2015/
doi:10.5194/bg-12-7453-2015

Biogeosciences Open Access EGU

Age–depth model of the past 630 kyr for Lake Ohrid (FYROM/Albania) based on cyclostratigraphic analysis of downhole gamma ray data

H. Baumgarten[1], T. Wonik[1], D. C. Tanner[1], A. Francke[2], B. Wagner[2], G. Zanchetta[3], R. Sulpizio[4], B. Giaccio[5], and S. Nomade[6]

[1]Leibniz Institute for Applied Geophysics, Section Rock Physics & Borehole Geophysics, Hanover, Germany
[2]University of Cologne, Institute for Geology and Mineralogy, Cologne, Germany
[3]University of Pisa, Dipartimento di Scienze della Terra, Pisa, Italy
[4]University of Bari Aldo Moro, Dipartimento di Scienze della Terra e Geoambientali, Bari, Italy
[5]Instituto di Geologia Ambientale e Geoingegneria – CNR, Rome, Italy
[6]Laboratoire des Sciences du Climat et de l'Environnement, IPSL, laboratoire CEA/CNRS/UVSQ, Gif-Sur-Yvette, France

Correspondence to: H. Baumgarten (henrike.baumgarten@liag-hannover.de)

Received: 18 February 2015 – Published in Biogeosciences Discuss.: 22 May 2015
Revised: 2 December 2015 – Accepted: 3 December 2015 – Published: 17 December 2015

Abstract. Gamma ray (GR) fluctuations and potassium (K) values from downhole logging data obtained in the sediments of Lake Ohrid from 0 to 240 m below lake floor (b.l.f). correlate with fluctuations in δ^{18}O values from the global benthic isotope stack LR04 (Lisiecki and Raymo, 2005). GR and K values are considered a reliable proxy to depict glacial–interglacial cycles, with high clastic input during cold and/or drier periods and high carbonate precipitation during warm and/or humid periods at Lake Ohrid. Spectral analysis was applied to investigate the climate signal and evolution over the length of the borehole. Linking downhole logging data with orbital cycles was used to estimate sedimentation rates and the effect of compaction was compensated for. Sedimentation rates increase on average by 14 % after decompaction of the sediment layers and the mean sedimentation rates shift from 45 cm kyr^{-1} between 0 and 110 m to 30 cm kyr^{-1} from 110 to 240 m b.l.f. Tuning of minima and maxima of gamma ray and potassium values versus LR04 extrema, in combination with eight independent tephrostratigraphical tie points, allows establishing of a robust age model for the downhole logging data over the past 630 kyr.

1 Introduction

Lake Ohrid is located at the border between the former Yugoslav Republic of Macedonia (FYROM) and Albania (40°70′ N, 20°42′ E) in the central Mediterranean region (Fig. 1a). It is considered as one of the oldest, continuously existing lakes worldwide. Its sediments are assumed to contain the climate history over more than 1 million years and numerous endemic species have evolved in Lake Ohrid. Several pre-site studies between 2004 and 2012, such as multichannel seismic and shallow coring, demonstrated the potential of Lake Ohrid to yield a complete and continuous palaeoclimatic record (e.g. Wagner et al., 2008; Lindhorst et al., 2015). Hydroacoustic data obtained by multichannel airgun and sediment echosounder seismics revealed undisturbed sediments as well as certain high-amplitude reflectors, which were interpreted as tephra layers (Lindhorst et al., 2015). A successful deep drilling campaign by the International Continental Scientific Drilling Program (ICDP) was performed in 2013. At the main drill site, the "DEEP site" in the central deep basin of Lake Ohrid (Fig. 1b), multiple coring and downhole logging tools were applied.

The reconstruction of Lake Ohrid's climatic, tectonic, and evolutionary biological history is one of the key objectives of the project Scientific Collaboration on Past Speciation Conditions in Lake Ohrid (SCOPSCO). This requires a reliable

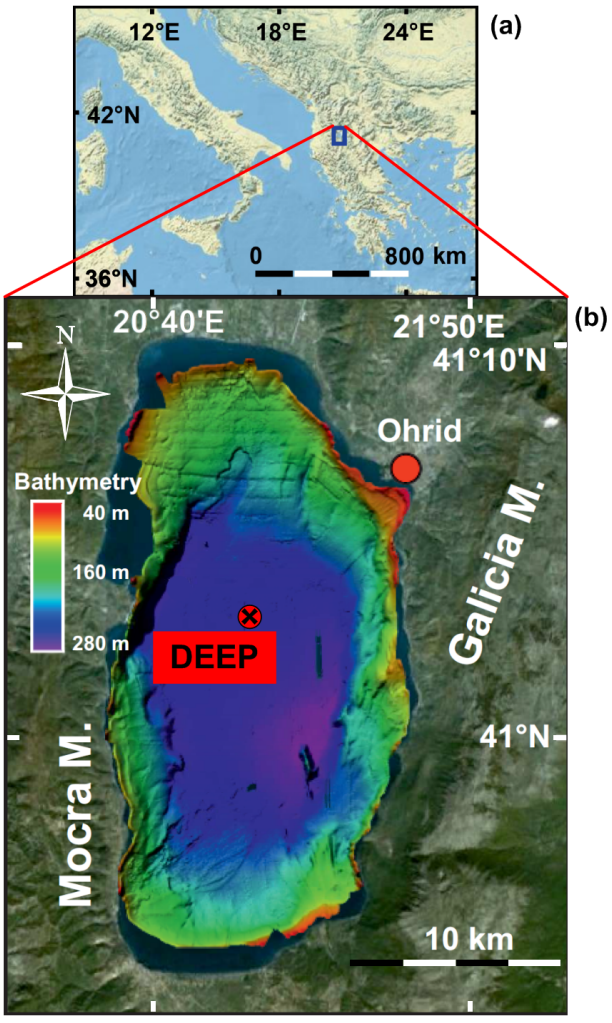

Figure 1. (a) Regional map of Lake Ohrid in the Mediterranean region and **(b)** bathymetric map of the lake. The city of Ohrid and the DEEP drill site from the ICDP campaign are shown (modified after Wagner et al., 2014).

temporal framework of the biotic and abiotic events and thus the establishment of a robust age–depth model. This can be achieved by tephrostratigraphy (Sulpizio et al., 2010; Vogel et al., 2010c), the use of radiometric ages (e.g. from dating of volcanic material in the cores), or by tuning proxy data, such as δ^{18}O or TOC, to reference records (Lang and Wolff, 2011; Stockhecke et al., 2014). Suitable material for independent dating, e.g. well-preserved and coarse-grained tephra layers, is often rare or hard to detect in sediments. Even if age control points are available, changes in the sedimentation rate between these points remain an uncertain interpolation. Amongst proxy data, the effect of global climate signals (Milanković cycles; Milanković, 1920) can be used to construct the temporal framework of a sedimentary record (Batenburg et al., 2012; Prokopenko et al., 2006; Wu et al., 2012). These cycles have periodicities of 100 kyr (eccentricity; E), 41 kyr (obliquity; O), and 23 and 19 kyr (precession; P_2, P_1) and determine the intensity of the solar insolation on Earth, whereas their effect is non-uniform and depends on the location of a certain site (e.g. the effect of O is strongest at polar regions) (Pälike, 2005). The 100 kyr cycle dominates the past ca. 900 kyr (Berger and Loutre, 2010), which is evident in sedimentary records and strongly imprinted in the widely used global climate reference record (LR04 stack from benthic foraminifera δ^{18}O) (Lisiecki and Raymo, 2005, 2007). To apply cyclostratigraphic methods successfully, generation and preservation of cycles is required, as well as their continuous recording. Such conditions are favoured in marine environments and ice cores, which are commonly used to analyse cyclicities (Barthes et al., 1999; Golovchenko et al., 1990; Jarrard and Arthur, 1989; Jouzel et al., 2007; Molinie and Ogg, 1990a). However, several lacustrine sequences have also recorded global climate signals and have been used for cyclostratigraphic studies (Baumgarten and Wonik, 2015; Bogota-A et al., 2011; Nowaczyk et al., 2013; Prokopenko et al., 2006). Whereas the majority of studies were performed on proxies from sediment cores (e.g. δ^{18}O, organic matter, or pollen), analysis of physical properties from downhole logging have also been successful (Barthes et al., 1999; Golovchenko et al., 1990; Jarrard and Arthur, 1989; Molinie and Ogg, 1990b; Wonik, 2001).

Physical in situ properties can be only achieved by downhole logging methods and provide a first data set that is available within hours after the tools are run in hole. Contrasting physical properties and therefore changes in the sediment characteristics (e.g. sedimentological composition, grain size) can trigger cyclic changes in the logging data (Baumgarten and Wonik, 2015; Kashiwaya et al., 1999; Paulissen and Luthi, 2011; Scholz et al., 2011). Such cyclic changes can potentially be revealed by applying cyclostratigraphic methods. The aim of this study is the generation of a robust age–depth model down to 240 m below lake floor (m b.l.f.) by an integrated study of downhole data with tephrostratigraphic age control from the sediment cores. Special emphasis is given to the effect of compaction and its subsequent impact on estimates of sedimentation rates. Furthermore, the response of the physical in situ properties from spectral gamma ray (contents of potassium, thorium, and uranium) and their application as proxy for changing environmental conditions in the catchment area is investigated.

2 Setting and sediment dynamics of Lake Ohrid

Lake Ohrid is located on the Balkan Peninsula at an altitude of 693 m above sea level in a northwest-trending active tectonic graben. It is considered to have formed within a first stage in the Late Miocene as a pull-apart basin and during a second stage in the Pliocene by E–W extension which led to the recent geometry (Lindhorst et al., 2015). The lake is considered be the oldest continuously existing lake in Europe, as

supported by molecular clock analysis, which estimates the onset of the lake formation to be 1.5 to 3 Ma (Trajanovski et al., 2010; Wagner et al., 2014). It houses an extraordinary number of endemic species (> 200, e.g. ostracodes), and it is therefore considered to be a hotspot to study the evolution of the various species (Albrecht and Wilke, 2008).

Oligotrophic Lake Ohrid has a surface area of 360 km^2 and a water depth of up to 290 m. The water originates mainly from karst inflows (50 %), precipitation (25 %), and surface runoff (25 %). The karst springs are primarily fed by the "sister lake" Prespa, 150 m higher in elevation (Wagner et al., 2014). The recent local climate is characterized by warm dry summers (mean temperature 26 °C) and cold winters (−1 °C). The annual precipitation is about 750 mm and winds are prevailing southerly or northerly, which is topographically controlled by the shape of the lake basin (Vogel et al., 2010a).

Due to its downwind location of most of the Quaternary volcanoes of central-southern Italy, Lake Ohrid's sediments can provide a record of the volcanic history of the northern Mediterranean region (Sulpizio et al., 2010). The catchment area southeast and northwest of the lake mostly consists of Triassic carbonates and clastics, whereas ophiolites (nickel-, iron-, and chromium-bearing) are exposed on the western and southwestern shore (Vogel et al., 2010b).

The sediment dynamics for the past 150 kyr have been investigated by up to 15 m long sediment cores from different marginal parts of the lake basin (e.g. Wagner et al., 2009, Belmecheri et al., 2009, Vogel et al., 2010a). Two major lithofacies are distinguished: A, sediments with high detrital clastic content with no or very low carbonate content, together with low organic matter and few diatoms, and B, sediments with high content of carbonates, abundant ostracodes, minor amounts of clastics, and high contents of organic matter. Lithofacies A is associated with glacial conditions (marine isotope stages: MIS 2, 4, 6), high clastic supply, and low lake productivity, whereas lithofacies B formed during interglacial conditions (mainly during MIS 1 and 5), with high lake productivity and formation of authigenic carbonates. Age control of the last glacial cycle was obtained by radiocarbon dating and tephrochronology.

3 Methods and background

3.1 Downhole logging data acquisition and processing

The multiple-cored DEEP site has six parallel and overlapping boreholes (A to F), of which holes A and E only cover the uppermost few metres of the sediment succession. Each of the deeper holes was drilled with a diameter of 149 mm and water-based mud was used to clean the holes of cuttings and to stabilize the side walls during the coring process. Hole C was logged immediately after drilling down to 470 m b.l.f., and amongst other probes, such as a resistivity and borehole televiewer, a spectral gamma ray (SGR) and sonic probe were used. To prevent the unconsolidated sediments from caving in, the SGR probe was run through the drill pipe and a continuous record of the sediments down to 470 m b.l.f. was achieved. The SGR data were acquired using the SGR 70-slimhole tool of the Leibniz Institute for Applied Geophysics (LIAG), which records the total gamma radiation (GR), as well as the spectral components (potassium, K; thorium, Th; and uranium, U) and their contribution to the GR. The tool was run at a logging speed of 3 m min^{-1} and a sampling rate of 10 cm. The achievable minimum bed resolution is controlled by the size of the bismuth germanate crystal (5 × 15 cm) and the characteristics of the target formation such as the absolute value range and contrast of values between neighbouring beds (Theys, 1991). The vertical resolution is estimated to 15–20 cm. The sonic tool, which measures the seismic velocity (V_p), was applied afterwards at a speed of 4 m min^{-1} and a depth increment of 10 cm. To allow open-hole measurements by sonic logging, the drill pipes were successively pulled upwards until open hole sections of ca. 50 m were accessible. The uppermost 30 m b.l.f. could not be logged by the sonic tool, because some drill pipes were kept in hole to allow other probes to enter. The measuring principles are described by Rider and Kennedy (2011) and the tools are specified in Buecker et al. (2000) and Barrett et al. (2000). The data were acquired, preprocessed, and processed with the software GeoBase® (Antares, Germany) and WellCAD® (Advanced Logging Technology, Luxembourg).

3.2 Sliding window method

Sedimentary cycles in lake records can be studied by cyclostratigraphic methods for a potentially orbitally driven origin (Lenz et al., 2011; Prokopenko et al., 2001; Weedon, 2003). To investigate wavelengths and amplitude of the contained signals, fast Fourier transform (Weedon, 2003) can be applied. The sliding window method (windowed Fourier transform) (Baumgarten and Wonik, 2015; Molinie and Ogg, 1990b; Torrence and Compo, 1998; Weedon, 2003) can be applied to identify the distribution of cycles within a series and their evolution over the data set: the spectral analysis is calculated for a depth interval of specific length (window size) and the resulting spectrum is allocated to the centre of the window. Subsequently, the window is moved downwards by a certain step size and the analysis is repeated at consecutive depth positions until the window border reaches the end of the data set. The results are presented in a three-dimensional spectrogram with colour coding of the relative power of the different frequency components. Generally, a small window size is favourable to maximize the length of the resulting plot. However, the contained cycle needs to be covered and cannot be determined if the window size was chosen too short, e.g. only half the signal's wavelength. The optimal window size is determined by empirical testing. Spectral analysis for identification of the characteristic peri-

odicities (Jenkins and Watts, 1969; Priestley, 1981) was performed on normalized SGR data using fast Fourier transform within MATLAB (MathWorks®).

The detection of cycles by SGR logging is limited by the Nyquist frequency, which is twice the sampling rate (Molinie and Ogg, 1990a). The temporal resolution can be estimated by the vertical resolution of the applied tools and the averaged sedimentation rate. For a mean sedimentation rate of, for example, 38 cm kyr^{-1}, cycles in the range of 0.8 to 1.1 kyr are resolvable by SGR logging.

3.3 Depth matching of downhole logging and core data

In this study, downhole logging data, in conjunction with stratigraphically aligned tephra layers in the cores, is used to construct an age–depth model. Therefore, matching of core and logging depth is required. To provide age control by distinct tephra layers, the layers need to be identified in the cores by visual description or by their physical properties, such as susceptibility from core logging, in contrast to the background sediments. Artifacts in the coring process, such as incorrect depth allocation of coring tools or gas extension of sediments due to pressure release, produce erroneous depth. Furthermore, depth shifts between core and logging depth are generated because the downhole data originate from one hole (C; down to 470 m b.l.f.) and the core composite record (see Francke et al.; 2015) is composed of four different holes which are tens of metres apart. The depth of a distinct sediment layer may differ up to 3 to 4 m between these holes. The matching of borehole logging data and sediment core is described in detail in Francke et al. (2015) and based on a correlation of K contents from SGR with K intensities from X-ray fluorescence (XRF) scanning, and using magnetic susceptibility from downhole logging and multi-sensor core logging (MSCL) on sediment cores. Trends and patterns were compared and matched; the larger features were preferred over correlation of small-scale features in the data. Cross correlation was used to prevent systematic depth shifts of these data sets and for quality control.

3.4 Compaction

To perform cyclostratigraphic studies and to estimate an age–depth relationship and sedimentation rates, compaction and associated reduction of sediment thickness due to overburden pressure must be considered. The original (decompacted) thickness of the sediments can be calculated if the initial (surface) porosity and the compaction coefficient (Brunet, 1998) can be determined. The amount of porosity decrease with greater depth depends on sediment properties, such as grain size and sorting (Serra and Serra, 2003), and can be expressed as

$$\Phi(z) = \Phi_0 \cdot e^{(-cz)}, \quad (1)$$

where the porosity (Φ) at a specific depth (z) is to be estimated; Φ_0 is the initial porosity and c is the compaction coefficient (Athy, 1930; Brunet, 1998).

Porosity can be measured directly on the sediment cores, e.g. by Archimedean weighing. However, the physical properties, in particular from (unconsolidated) sediment cores, are typically disturbed due to drilling, release of pressure, and core handling. Therefore, measurements by downhole logging are more suitable; in situ porosity can be gained by neutron porosity logging or derived, e.g. from bulk density. These tools operate with radioactive methods and the import procedure into foreign countries is usually extremely complicated and seldom successful. Therefore, the radioactive tools from the LIAG could not be used at Lake Ohrid. However, porosity was derived by an empirical relationship from sonic data (V_p) (Erickson and Jarrard, 1998), which were recorded continuously from below 30 m b.l.f. The software 2DMove® (Midland Valley Exploration Ltd.) was used to decompact the sediments and calculate the original sediment thickness.

4 Results

4.1 Selection of SGR data

The output curves from SGR were compared to estimate the contribution of the spectral components to the total gamma ray. GR is mainly controlled by K and Th, which develop uniformly ($R > 0.9$). GR and K were used for further investigations. K was chosen over Th, because it is also available from XRF core scanning and the interpretation can be reviewed easily.

4.2 Correlation of GR with the global climate reference δ^{18}O record

The downhole logging data (GR and K) from 0 and 240 m b.l.f. was compared to the global benthic isotope stack LR04 (Lisiecki and Raymo, 2005). In order to select an appropriate temporal window, we considered the current age estimates from stratigraphical aligned tephra layers (eight age–depth points; Table 1). After the anchor points from tephra deposits were defined, significant variations in the data were correlated; a very similar cyclicity with a positive correlation between GR and K from downhole logging data and δ^{18}O data was observed (Fig. 2a). The onset and terminations of several marine isotope stages can be easily distinguished in the downhole logging data, whereas warm and/or humid periods (decreased δ^{18}O values) correlate with low GR values. Thirty additional tie points (Table 1) were set due to the strong similarities between the curves characteristics. After matching these tie points, high correlation of both data sets ($R = 0.75$) was observed. The tephra ages and tie points from correlation between GR, K, and LR04 were used to assign a (preliminary) timescale to the data (Fig. 2b). Within the data, the timescale between the tie points was generated by

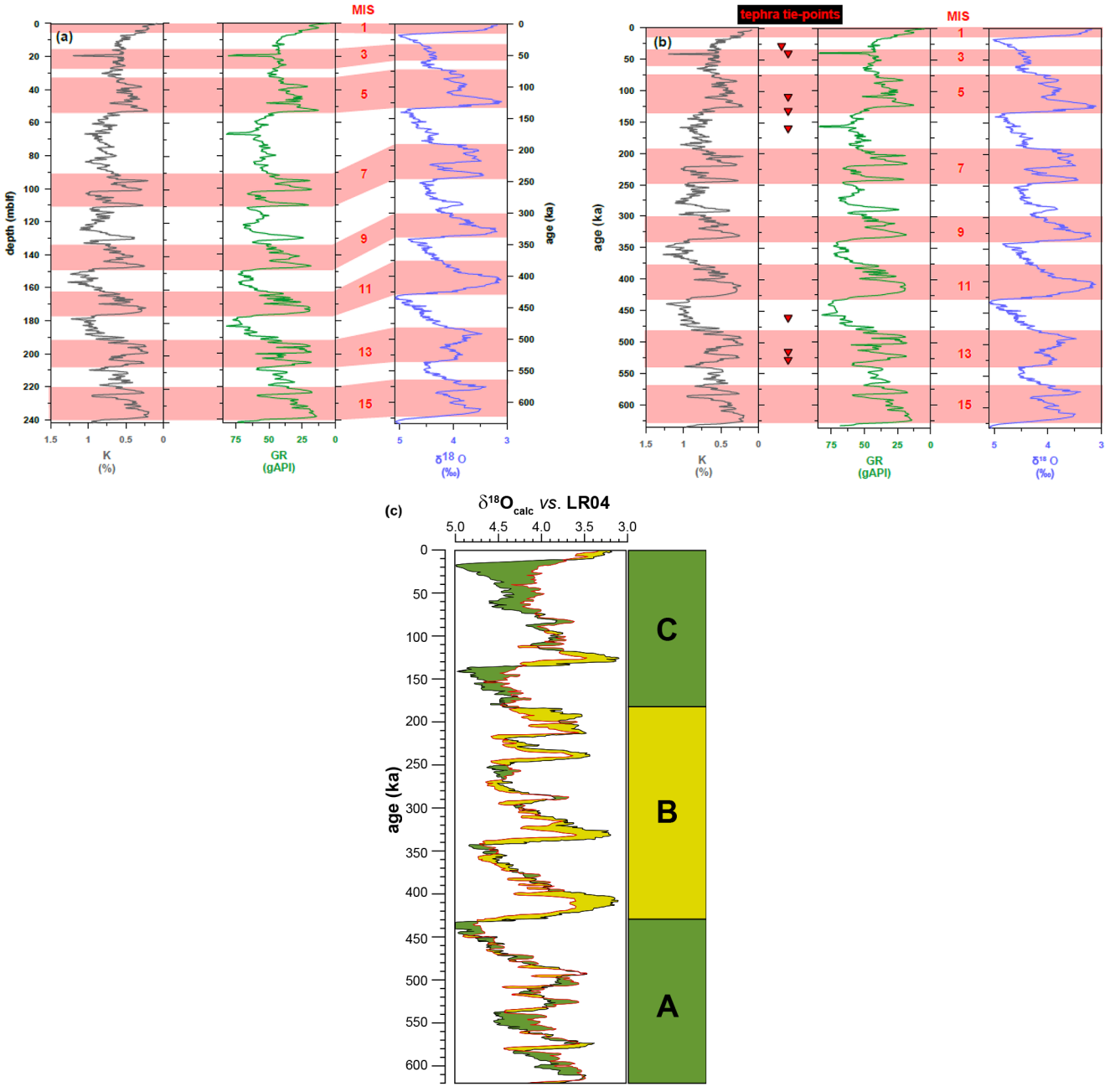

Figure 2. (a) Correlation of downhole GR and K data from 0 to 240 m b.l.f. with LR04 (Lisiecki and Raymo, 2005) from 0 to 630 ka. The age–depth range was set by eight anchor points from tephrochronology. Warm and/or humid periods correlate with periods of low GR and K values. **(b)** An age scale was applied to the downhole logging data (GR and K) based on tie points to LR04 (Lisiecki and Raymo, 2005) and from tephrochronology. **(c)** A synthetic curve calculated by linear regression between GR on timescale and LR04. Both curves are displayed as overlay and three zones are identified. A: 630 to 430 ka (MIS 15 to 12); B: 430 to 185 ka (MIS 11 to 7); C: 185 to 0 ka (MIS 6 to 1). $\delta^{18}O_{calc}$ is prevailing decreased during zones A and C (dark-green colour) and higher in zone B (light-green colour) compared to LR04. K – potassium content from spectral gamma ray; GR – total gamma radiation; MIS – marine isotope stage; m b.l.f. – metres below lake floor.

linear interpolation. According to the established age model, the 240 m long sediment succession covers a time period between 630 ka (including MIS 15) and the present.

The conspicuous similarity of the data sets allows calculation of a synthetic $\delta^{18}O$ curve from GR by a regression of both data sets. Therefore, normally distributed data are required and thus the prominent tephra layers at 20 and 68 m b.l.f. (Fig. 2c) were considered to be outliers and removed. Best results were achieved by a linear solution ($R^2 = 0.60$) as follows:

$$\delta^{18}O_{calc}(‰) = 3.19 + 0.03 \cdot GR.(gAPI) \quad (2)$$

Whereas cycles and trends are similar in both data sets, the amplitudes between the LR04 stack and the synthetic $\delta^{18}O$ (derived from GR; $\delta^{18}O_{calc}$; Fig. 2c) do not completely match. The $\delta^{18}O_{calc}$ values from 630 to 430 ka are lower than compared to LR04. From 430 to 185 ka the amplitude of $\delta^{18}O_{calc}$ is higher and during the past 185 kyr, $\delta^{18}O_{calc}$ is mostly decreased compared to LR04. These three zones (A to C) are indicated in Fig. 2c.

4.3 Spectral characteristics of GR data, temporal evolution, and sedimentation rates

After visual comparison of GR and K with LR04 documenting a strong correlation of periods with low GR and K with warm and/or humid periods, the application of spectral analysis by sliding window analysis objectively identifies the possible cycles and their temporal distribution. The spectral analysis was calculated with a window of 90 m length and a step size of 1 m. Thus, the stepwise calculation for the depth section from 0 to 240 m b.l.f. and the resulting three-dimensional spectral plot (Fig. 3a) is composed of 150 spectra. The plot ranges from 45 to 240 m b.l.f., because the first spectrum is allocated to the window centre (Sect. 3.2) and therefore half of the window length is not displayed. Two prominent spectral peaks are evident in the data set, as indicated by colour with wavelengths of 30 and 45 m. The distribution of the cycles is non-uniform along the data set and a break in the spectral characteristics occurs at about 110 m b.l.f. Based on the reduced relative power of the 30 m signal and the subsequent increased power of the 45 m frequency at 110 m b.l.f., the plot can be split into a lower interval I and an upper interval II (Fig. 3a). In addition, two single spectra from depths of 170 and 50 m b.l.f. (Fig. 3b, c) are displayed.

The similar cyclicity in the LR04 stack and GR (Fig. 2a, b) suggests that the 100 kyr cycle, known as dominant periodicity in sedimentary archives for the past ca. 900 kyr and clearly documented in the $\delta^{18}O$ data, has the strongest effect on the cyclic characteristics of the GR data. The highest amplitudes were therefore linked to the 100 kyr cycle. Averaged sedimentation rates can be calculated using this link (45 m ≡ 100 kyr cycle) for 110 to 0 m b.l.f. as follows:

$$45\,m/100\,kyr = 45\,cm\,kyr^{-1}. \quad (3)$$

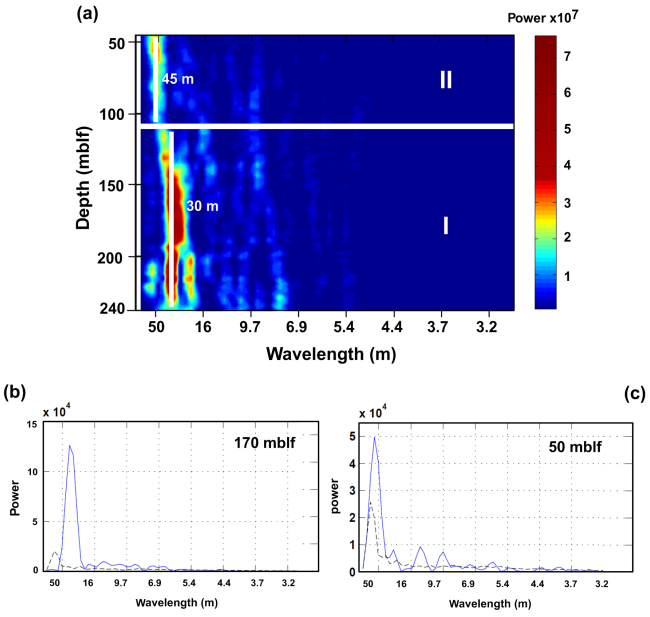

Figure 3. (a) Three-dimensional spectrogram from sliding window analysis of GR data from 0 to 240 m b.l.f. The relative power of the frequency components is indicated by colour and two spectral peaks with wavelengths of 30 and 45 m are apparent. Based on the break in the spectral characteristics at about 110 m b.l.f., the spectral plot was subdivided into a lower interval I (240 to 110 m b.l.f.) and an upper interval II (110 to 0 m b.l.f.). Single spectra of GR from interval I at 170 m b.l.f. **(b)** and from interval II at 50 m b.l.f. **(c)** are displayed below and show that the wavelengths of 30 and 45 m are prominent. The dashed line separates the spectral background from the spectral peaks.

Furthermore, the time of deposition can be estimated by using this sedimentation rate and the length of the interval II (length of 110 m):

$$110\,m/45\,cm\,kyr^{-1} = 244\,ka. \quad (4)$$

The sedimentation rate for interval I (length of 130 m) can be calculated as 30 cm kyr^{-1} (30 m ≡ 100 kyr cycle). Thus, for interval I the duration of deposition of 433 ka is calculated, which gives an overall time of deposition (sum of interval I and II) of 677 ka.

The sedimentation rates from sliding window analysis show a distinct shift from 30 to 45 cm kyr^{-1} at 110 m b.l.f. (Fig. 4). However, the sedimentation rates from visual tying to LR04 are more variable and range from 22 to 71 cm kyr^{-1}. Exceptionally high sedimentation rates occurred during MIS 6 and lowest sedimentation rates occurred during MIS 11 and 13. The sedimentation rates from LR04 tie points were averaged over the length of the intervals and show mean values of 35 cm kyr^{-1} for interval I and 48 cm kyr^{-1} for interval II (Fig. 4).

Table 1. Downhole logging data correlated to LR04 (Lisiecki and Raymo, 2005). Eight anchor points from tephrochronology (Leicher et al., 2015) and 30 additional tie points of significant features between the downhole data and LR04 are set. The tephra ages were recalculated (except Y-3) according relative to ACs-2 at 1.193 Ma (Nomade et al., 2005) and the total decay constant of Steiger and Jäger (1977), uncertainties are 2δ. m b.l.f. – metres below lake floor.

Depth m b.l.f.	Age from LR04 tie points ka	Age from tephra tie points ka	Correlated eruption/tephra	Reference
1.46	4			
13.67		29	Y-3	Albert et al., 2014
19.35		39	Y-5 (Campanian Ignimbrite)	De Vivo et al. (2001)
24.37	49			
30.17	62			
36.41	78			
40.10	87			
48.40		109 ± 2	X-6	Iorio et al. (2013)
55.11		129 ± 6	P11	Rotolo et al. (2013)
59.19	140			
66.73		162 ± 6	Vico B	Laurenzi and Villa (1987)
74.61	171			
85.09	185			
97.00	206			
103.40	223			
106.48	230			
112.10	246			
121.75	271			
132.92	294			
144.00	317			
150.65	342			
153.76	350			
161.52	374			
167.80	392			
170.04	398			
178.29	433			
183.28	456	457 ± 2	Pozzolane Rosse	Giaccio et al. (2013)
201.31	508			
203.05		511 ± 6	Acerno A10-A9	Petrosino et al. (2014)
206.70		527 ± 2	Tufo Bagni Albule	Marra et al. (2009)
209.09	536			
212.89	549			
215.53	557			
219.20	568			
220.99	574			
225.44	585			
240.00	630			

4.4 Decompaction of the pelagic sediments and subsequent spectral analysis on GR data on decompacted depth scale

The effect of decreased sediment thicknesses due to compaction over time was determined to investigate its impact on the estimates of sedimentation rates. The V_p data from sonic logging were used to derive porosity after Erickson and Jarrard (1998). The porosity values were averaged for layers of 100 m thickness (Fig. 5a). The initial porosity (Φ_0) was determined at 80 % and the compaction coefficient was estimated at $0.39\,km^{-1}$. These parameters were used as input data for modelling decompaction of the sediments, and the 2-D model was calculated for layers of 50 m thickness. The modelling process starts with the removal of the top layer and subtraction of its overburden pressure. The new thicknesses of the lowermost layers are thereafter calculated and these steps were repeated again downwards. The resulting thicknesses of the sediment layers after decompaction show a quasi-linear increase with greater depth for these small depths (Fig. 5b). Decompaction of the sediment layers ranges from 10 to 30 % downwards and the cumulative thickness

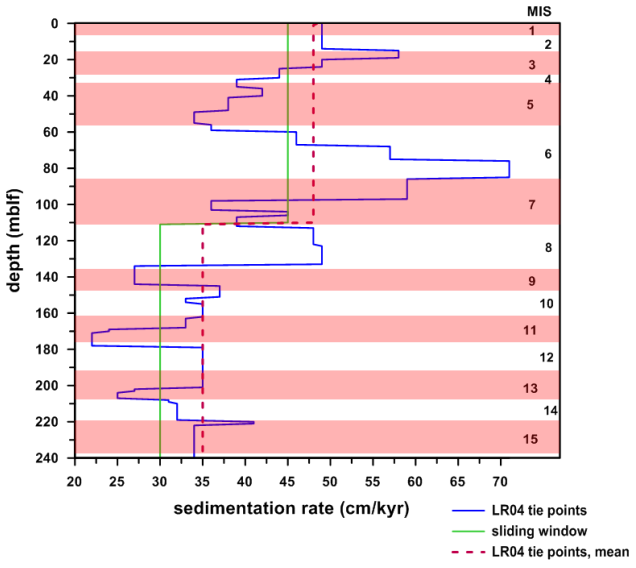

Figure 4. Estimates of sedimentation rates from 0 to 240 m b.l.f. based on visual correlation and tying to the timescale of LR04 (blue; Lisiecki and Raymo, 2005) and sliding window analysis with linking of high amplitudes to the 100 kyr cycle (green). The sedimentation rates from sliding window analysis show an increase from 30 to 45 cm kyr^{-1} at about 110 m b.l.f., whereas results from tie points are more variable and range from 22 to 71 cm kyr^{-1}. The dashed red line indicates the mean values of the sedimentation rates from LR04 tie points for interval I and II. Marine isotope stages (MIS) from 1 to 15 are labelled.

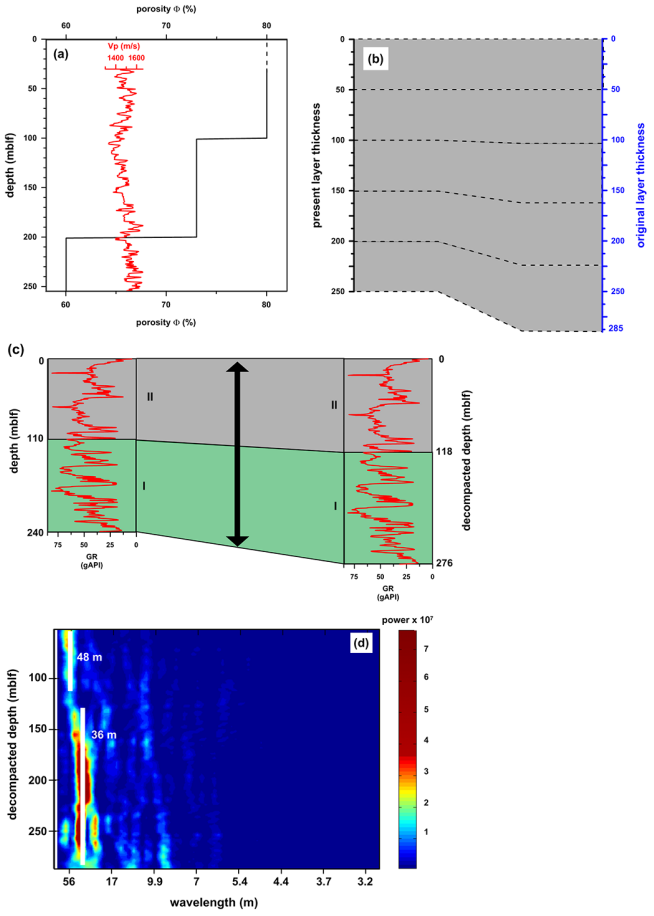

Figure 5. (a) Porosity values derived from sonic (V_p) after Erickson and Jarrard (1998) from 30 to 250 m b.l.f. Average values for intervals of 100 m length were calculated as indicated by the black line and values for the top 30 m of the sediments were linear interpolated (dashed black line). An initial porosity (surface porosity) of 80 % was used for modelling of compaction by 2DMove. Φ – porosity; V_p – p wave velocity from sonic. **(b)** Sediment layers of thicknesses of 50 m are modelled applying the software 2DMove. The cumulative present layer thickness of 250 m is extended after decompaction to 285 m (original layer thickness). **(c)** The GR data from 0 to 240 m b.l.f. and the intervals from subdivision by spectral characteristics at about 110 m b.l.f. (left). The data were stretched to the estimates of the original layer thickness. The decompacted depth and new interval borders are displayed (right). **(d)** Result from sliding window analysis of GR data on decompacted depth scale. Two spectral peaks with wavelengths of 36 and 48 m are emphasized. GR – gamma ray; m b.l.f. – metres below lake floor.

of the sediment sequence (present thickness of 250 m) is increased by 35 m (to 285 m).

The GR data were stretched (Fig. 5c) and subsequently spectrally analysed by sliding window method (Fig. 5d) to determine the effect of decompaction on the spectral analysis. The spectral analysis shows two spectral peaks (Fig. 5d; wavelength of 36 m from 276 to 118 m and wavelength of 48 m from 118 to 0 m). Linking these spectral peaks to the 100 kyr cycle provided sedimentation rates of 36 cm kyr^{-1} for interval I and 48 cm kyr^{-1} for interval II. Times of deposition remain constant and are 433 ka for interval I and 244 ka for interval II.

5 Discussion

5.1 Climate response of GR over the past 630 kyr

The strong correlation of GR and K with LR04 (low GR and K during warm and/or humid periods, high in cold and/or drier periods) suggests a response of the sedimentary system to the temperature and hydrological changes related to the global ice-volume fluctuations during the glacial–interglacial cycles. The fluctuations are likely to be controlled by the input and deposition of clastics (K and Th sources), which are suggested to have increased during the past ca. 136 kyr, when glacial conditions prevailed (except MIS 1 and 5e) at Lake Ohrid (Vogel et al., 2010a). In particular, the reduced input of organic matter and calcium carbonate during cold and/or drier periods seems to amplify the enhanced input of clastic material. During warm and/or humid periods, carbonate production and preservation is increased (Vogel et al., 2010a). In combination with higher organic matter flux, the clastic content of the sediments is reduced and the GR and K data

are lower. Either the total content of clastics is lower during warm-humid periods or the amount is decreased relative to carbonate and organic matter (diluted). However, as discussed by Vogel et al. (2010a), less vegetation cover during cold and drier periods is likely and also suggests increased erosion in the catchment and subsequent higher input of clastic material. Based on our interpretation, these cyclic changes from carbonate-rich to clastic-rich sedimentation were constant at least for the past 630 kyr.

Three zones were observed, based on amplitude differences between the synthetic $\delta^{18}O$ curve from GR ($\delta^{18}O_{calc}$) and the referenced record: A, 630 to 430 ka (MIS 15 to MIS 12); B, 430 to 185 ka (MIS 11 to MIS 7); C, 185 to 0 ka (MIS 6 to MIS 1). Comparison of the synthetic $\delta^{18}O_{calc}$ to LR04 revealed systematically lower values in zones A and C and higher values in zone B.

We suggest the following reasons of the GR signature:

1. Climate-dependent supply and deposition of K-rich clastics (feldspars, clays). They are increased during cold, dry periods (high GR) and decreased during warm, wet periods (high carbonate deposition; low GR) in the sediments.

2. Tephra layers that are partly recognizable in the GR/K data (increased GR). Even if the prominent layers at 20 and 68 m b.l.f. could be removed, at least 6 additional tephra layers (see tephra tie points; Fig. 2b) were identified in the cores down to 240 m b.l.f. These thin layers (thickness < 10 cm) are not recognizable easily in the GR data and could not be removed but are assumed to contribute to the GR/K curve. Their occurrence in zones A and C (Fig. 2c; zones of decreased synthetic $\delta^{18}O$) suggests that they have an effect on the GR signature.

3. Variations in the catchment area. Outcrops of Triassic carbonates and clastics occur in large parts in Lake Ohrid's catchment area. Furthermore, ophiolites, magmatic, and metamorphic rocks are exposed and are potential sources of terrestrial material. Erosion and transport of these rocks, e.g. by means of surface runoff into the lake, and subsequently the input of K-bearing particles, were likely variable over time.

Therefore, the GR is most likely controlled by several factors and cannot be described in total by linear solution. However, the main component seems to be a linear response of K-rich sediments to the global climate trend (1). Further, we consider the attempt useful to compare both data sets and to show the very unusual similarity in cyclic characteristic between LR04 and GR.

Matching of GR and K data with the global climate reference record (LR04) equates the timing of the climate dynamics recorded in the oceans to Lake Ohrid. This means that if the downhole logging data are tied to this timescale, differences between the response times of Lake Ohrid and the global climate trend (e.g. lead or lag effects of the onset of terminations) are lost. However, even if the comparable small system was likely to be subject to a faster climate response compared to records from the marine realm, correlation with the global signal and the resulting age–depth model is verified in large parts (down to 206 m b.l.f.) by tephrochronology.

5.2 Sedimentation rates: major trends, small-scale fluctuations, and the effect of compaction

The relative power of the spectral peaks from sliding window analysis seems to be higher in interval I (wavelength of 30 m) in comparison to interval II (wavelength of 45 m). The strength of the signal depends on the number of cycles that are detected by spectral analysis. The 45 m long cycle can be contained up to 2.4 times in the 110 m long interval II, whereas the cycle of wavelength of 30 m might be recorded more frequently (4.3 times) in the 130 m long interval I. This can contribute to the higher intensity of the 30 m amplitude and thus we cannot interpret a stronger cyclicity for the lower part.

Based on sliding window analysis, the sedimentation rates are constant (30 cm kyr^{-1}) for a long period of time (433 kyr), apart from a shift to increased rates at about 110 m b.l.f. to 45 cm kyr^{-1}. However, small-scale variations cannot be resolved due to averaging and the window of 90 m length used. More variable and realistic results are indicated by tying of GR and K to LR04. The lowest rates (minimum of 22 cm kyr^{-1}) occur during MIS 13, 11, and 9. Strongly increased sedimentation rates (up to 71 cm kyr^{-1}) occur during MIS 8 and in particular during MIS 6. Therefore, decreased sedimentation rates during interglacials and increased rates during glacial periods can be derived. Even if these fluctuations do not correlate with all MIS, they seem to be largely coupled to glacial–interglacial dynamics. This trend suggests higher accumulation of clastic-rich glacial deposits compared to calcium carbonate-rich deposition during interglacials. The overall trend from lower mean rates in the bottom part (> 110 m b.l.f., sliding window; > 130 m b.l.f.; LR04 tie points) to increased values towards the top is comparable.

The cumulative time of deposition based on these sedimentation rates and corresponding sediment thicknesses range from 630 ka (LR04 tie points) to 677 ka (sliding window method) and are overall in a similar range (Fig. 6). We consider the estimated time of deposition from the tuning to LR04 to be of higher accuracy compared to the averaged estimates from sliding window analysis. The agreement with age estimates from cores, based on wiggle matching of (bio)geochemistry data, such as XRF scanning data, to LR04 and local insolation patterns (Francke et al., 2015), supports the age–depth model. Nonetheless, the sliding window method is useful to estimate averaged sedimentation rates and to provide complementary cyclic characteristics of the data. Whereas age control from tephrochronology is

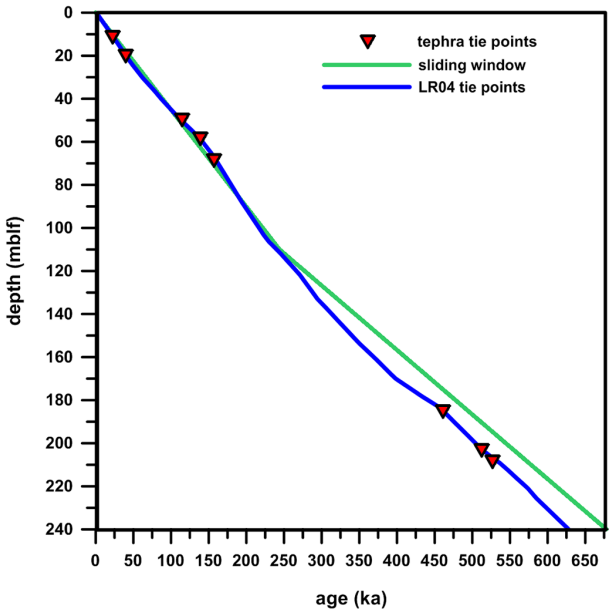

Figure 6. Age–depth model for the sediment depths of 0 to 240 m b.l.f. The two sedimentation rates were generated by visual tying to LR04 (blue line; Lisiecki and Raymo, 2005) and by linking of prominent cycles to the 100 kyr signal (green line). Tephra tie points are indicated by red triangles. m b.l.f. – metres below lake floor.

only available down to 206 m b.l.f., our interpretation was extended down to 240 m b.l.f. based on the constant cyclic characteristics.

The required initial porosity for modelling of the effect of compaction was derived from sonic logging ($\Phi_0 = 80\,\%$) and is commonly lower (at ca. 65 %) for sedimentary basins. Studies of physical properties of marine sediment cores have shown comparable values for seafloor deposits ($\Phi = 80\,\%$, $V_p = 1540\,\mathrm{m\,s^{-1}}$; Kim and Kim, 2001) and even higher porosity values (> 80 %; Kominz et al., 2011) for unconsolidated sediments. The compaction coefficient c was estimated at $0.39\,\mathrm{km^{-1}}$ and lies in the range between c used for sands ($0.20\,\mathrm{km^{-1}}$) and carbonates ($0.50\,\mathrm{km^{-1}}$) and thus is considered as reasonable. The overall trend of a quasi-linear evolution of decompaction with increasing depth was observed, although Eq. (1) describes an exponential curve, it can be approximated to a line over short lengths (< 500 m). This is in accordance with the average linear increase in V_p with greater depth. The tephra layers, with thicknesses of only a few centimetres, are considered to have little impact on the compaction of these sediments.

Spectral analysis of GR data on decompacted depth scale (Fig. 5c) revealed a very similar spectral characteristic compared to the sliding window plot of the compacted data. However, the two spectral peaks (wavelengths of 30 and 45 m) are shifted to higher wavelengths and increased to wavelengths of 36 m for interval I and 48 m for interval II. Therefore, the sedimentation rates are increased accordingly to $36\,\mathrm{cm\,kyr^{-1}}$ and would be underestimated by 7 to 20 %, if they are not corrected for the effect of compaction. Underestimation of sedimentation rates from sliding window analysis is supported by comparison of results from LR04 tie points; the latter indicate generally higher sedimentation rates ($35\,\mathrm{cm\,kyr^{-1}}$, interval I; $48\,\mathrm{cm\,kyr^{-1}}$, interval II) and show very good agreement with the estimates of the effect of compaction.

To determine the time of deposition, two input quantities were used: (1) sedimentation rates and (2) the thickness of the sediment layer for which they apply. Due to the stretching of the data set, the resulting sedimentation rates and the length of the intervals are increased and thus the duration of deposition remains unchanged. Therefore, the effect of compaction on this calculation is negligible.

6 Conclusions

Can climatic indicators be derived from downhole logging, despite its limited vertical (and temporal) resolution and can these proxies be used to reconstruct a robust age–depth model?

The strong response to the global climate signal (LR04) suggests that the K contents reflect a cyclic change of undisturbed, continuous sedimentation. Conditions were constant over a long period of time and prevailing in balance with the global climate. To investigate the response of our data to the global climate trend, a synthetic $\delta^{18}O$ curve was generated that reveals minor deviations compared to LR04. The deviations could indicate either that the local climatic conditions were not fully in line with the global climate or that local processes in the sedimentary system changed over time.

Within two independent attempts, visual tying to the global reference LR04 record as well as spectral analysis by the sliding window method and linking of high amplitudes to orbital cycles, a similar result was achieved. To derive sedimentation rates from spectral analysis, the effect of compaction must be taken into account. Our results show that the use of the present thicknesses of the sediment layers underestimates sedimentation rates by an average of 14 %, which needs to be corrected for by decompaction. In conjunction with tephrochronology (Leicher et al., 2015) from the same core material, a robust age–depth model can be established.

This data set will play a crucial role for other working groups and will complement the age–depth model from core analysis (Francke et al., 2015). The combination of both of these age–depth models will provide the temporal framework, e.g. for refining of the seismo-stratigraphical model by Lindhorst et al. (2015) and contribute to the reconstruction of Lake Ohrid's climatic, tectonic, and evolutionary biological history to answer the main research questions of the SCOPSCO project.

Due to the successful construction of an age–depth model based on the GR and K data down to 240 m b.l.f., we are optimistic that the complete lacustrine sediment succession (down to 433 m b.l.f.) has high potential for cyclostratigraphic analysis and will provide a key component to determine Lake Ohrid's temporal framework.

Acknowledgements. The SCOPSCO Lake Ohrid drilling campaign was funded by ICDP, the German Ministry of Higher Education and Research, the German Research Foundation, the University of Cologne, the British Geological Survey, the INGV and CNR (both Italy), and the governments of the FYROM and Albania. Logistic support was provided by the Hydrobiological Institute in Ohrid. Drilling was carried out by Drilling, Observation and Sampling of the Earth's Continental Crust's (DOSECC) and using the Deep Lake Drilling System (DLDS). Special thanks are due to Beau Marshall and the drilling team. Ali Skinner and Martin Melles provided immense help and advice during logistic preparation and the drilling operation.

We thank the German Research Foundation for financial support for the downhole logging (WO 672/10-1). The acquisition of these high-quality data was only possible due to the great commitment of our technical staff, Thomas Grelle and Jens Kuhnisch. We thank Midland Valley Exploration Ltd for the use of 2DMove.

Edited by: F. Wagner-Cremer

References

Albert, P. G., Hardiman, M., Keller, J., Tomlinson, E. L., Smith, V. C., Bourne, A. J., Wulf, S., Zanchetta, G., Sulpizio, R., Müller, U. C., Pross, J., Ottolini, L., Matthews, I. P., Blockley, S. P. E., Menzies, M. A.: Revisiting the Y-3 tephrostratigraphic marker: a new diagnostic glass geochemistry, age estimate, and details on its climatostratigraphical context, Quaternary Sci. Rev., in press, doi:10.1016/j.quascirev.2014.04.002, 2014.

Albrecht, C. and Wilke, T.: Ancient Lake Ohrid: Biodiversity and evolution, Hydrobiologia, 615, 103–140, 2008.

Athy, L. F.: Density, porosity, and compaction of sedimentary rocks, AAPG Bull., 14, 1–24. 1930.

Barrett, P. J., Sarti, M., and Wise, S.: Studies from the Cape Roberts Project Ross Sea, Antarctica Initial Report on CRP-3 Terra Antartica 7, 19–56, 2000.

Barthes, V., Pozzi, J. P., Vibert-Charbonnel, P., Thibal, J., and Melieres, M. A.: High-resolution chronostratigraphy from downhole susceptibility logging tuned by palaeoclimatic orbital frequencies, Earth Planet. Sci. Lett., 165, 97–116, 1999.

Batenburg, S. J., Sprovieri, M., Gale, A. S., Hilgen, F. J., Hüsing, S., Laskar, J., Liebrand, D., Lirer, F., Orue-Etxebarria, X., Pelosi, N., and Smit, J.: Cyclostratigraphy and astronomical tuning of the Late Maastrichtian at Zumaia (Basque country, Northern Spain), Earth Planet. Sc. Lett., 359–360, 264–278, 2012.

Baumgarten, H. and Wonik, T.: Cyclostratigraphic studies of sediments from Lake Van (Turkey) based on their uranium contents obtained from downhole logging and paleoclimatic implications, Int. J. Earth Sci., 104, 1639–1654, doi:10.1007/s00531-014-1082-x, 2015.

Belmecheri, S., von Grafenstein, U., Namiotko, T., Robert, C. M., Andersen, N., Danielopol, D. L., Caron, B., Bordon, A., Regnier, D., Mazaud, A., Sulpizio, R., Zanchetta, G., Grenier, C., Tiercelin, J. J., Fouache, E., and Lezine, A. M.: Potential of Lake Ohrid for long palaeoclimatic and palaeoenvironmental records; the last glacial-interglacial cycle (140 ka), Eos, Transactions, American Geophysical Union 90, @AbstractPP14A-03, 2009.

Berger, A. and Loutre, M. F.: Modeling the 100-kyr glacial-interglacial cycles, Global Planet. Change, 72, 275–281, 2010.

Bogota-A, R. G., Groot, M. H. M., Hooghiemstra, H., Lourens, L. J., van der Linden, M., and Berrio, J. C.: Rapid climate change from north Andean Lake Fuquene pollen records driven by obliquity; implications for a basin-wide biostratigraphic zonation for the last 284 ka, Quaternary Sci. Rev., 30, 3321–3337, 2011.

Brunet, M.-F.: Method of quantitative study of subsidence, Oxford & IBH Publishing Company Pvt., New Delhi, India, 79–88, 1998.

Buecker, C. J., Jarrard, R. D., Wonik, T., and Brink, J. D.: Analysis of downhole logging data from CRP-2/2A, Victoria Land Basin, Antarctica; a multivariate statistical approach, Terra Antartica, 7, 299–310, 2000.

De Vivo, B., Rolandi, G., Gans, P. B., Calvert, A., Bohrson, W. A., Spera, F. J., and Belkin, H. E.: New constraints on the pyroclastic eruptive history of the Campanian volcanic Plain (Italy), Min. Pet., 73, 47–65, 2001.

Erickson, S. N. and Jarrard, R. D.: Velocity-porosity relationships for water-saturated siliciclastic sediments, J. Geophys. Res., 103, 30385–30406, 1998.

Francke, A., Wagner, B., Just, J., Leicher, N., Gromig, R., Baumgarten, H., Vogel, H., Lacey, J. H., Sadori, L., Wonik, T., Leng, M. J., Zanchetta, G., Sulpizio, R., and Giaccio, B.: Sedimentological processes and environmental variability at Lake Ohrid (Macedonia, Albania) between 640 ka and present day, Biogeosciences Discuss., 12, 15111–15156, doi:10.5194/bgd-12-15111-2015, 2015.

Giaccio, B., Arienzo, I., Sottili, G., Castorina, F., Gaeta, M., Nomade, S., Galli, P., and Messina, P.: Isotopic (Sr-Nd) and major element fingerprinting of distal tephras: an application to the Middle-Late Pleistocene markers from the Colli Albani volcano, central Italy, Quaternary Sci. Rev., 67, 190–206, 2013.

Golovchenko, X., O'Connell, S. B., and Jarrard, R. D.: Sedimentary response to paleoclimate from downhole logs at Site 693, Antarctic continental margin, Proceedings of the Ocean Drilling Program, Scientific Results, 113, 239–251, 1990.

Iorio, M., Liddicoat, J., Budillon, F., Incoronato, A., Coe, R. S., Donatella, D., Insinga, D., Cassata, W., Lubritto, C., Angelino, A., and Tamburrino, S.: Combined palaeomagnetic secular variation and petrophysical records to time constrain geological and hazardous events: an example from the eastern Tyrrhenian Sea over the last 120 ka, Global Planet. Changes, 113, 91–109, 2013.

Jarrard, R. D. and Arthur, M. A.: Milankovitch paleoceanographic cycles in geophysical logs from ODP Leg 105, Labrador Sea and Baffin Bay. Proceedings of the Ocean Drilling Program, Scientific Results, 105, 757–772, 1989.

Jenkins, G. M. and Watts, D. G.: Spectral analysis and its applications. San Francisco: Holden Day, 525 pp., 1969.

Jouzel, J., Masson-Delmotte, V., Cattani, O., Dreyfus, G., Falourd, S., Hoffmann, G., Minster, B., Nouet, J., Barnola, J.M., Chappel-

laz, J., Fischer, H., Gallet, J. C., Johnsen, S., Leuenberger, M., Loulergue, L., Luethi, D., Oerter, H., Parrenin, F., Raisbeck, G., Raynaud, D., Schilt, A., Schwander, J., Selmo, E., Souchez, R., Spahni, R., Stauffer, B., Steffensen, J. P., Stenni, B., Stocker, T. F., Tison, J. L., Werner, M., and Wolff, E. W.: Orbital and Millennial Antarctic Climate Variability over the Past 800,000 Years, Science, 317, 793–796, 2007.

Kashiwaya, K., Ryugo, M., Horii, M., Sakai, H., Nakamura, T., and Kawai, T.: Climato-limnological signals during the past 260,000 years in physical properties of bottom sediments from Lake Baikal, J. Paleolimnol., 21, 143–150, 1999.

Kim, G. Y. and Kim, D. C.: Comparison and correlation of physical properties from the plain and slope sediments in the Ulleung Basin, East Sea (Sea of Japan), J. Asian Earth Sci., 19, 669–681, 2001.

Kominz, M. A., Patterson, K., and Odette, D.: Lithology dependence of porosity in slope and deep marine sediments, J. Sediment. Res., 81, 730–742, 2011.

Lang, N. and Wolff, E. W.: Interglacial and glacial variability from the last 800 ka in marine, ice and terrestrial archives, Clim. Past, 7, 361–380, doi:10.5194/cp-7-361-2011, 2011.

Laurenzi, M. A. and Villa, I. M.: 40Ar/39Ar chronostratigraphy of Vico ignimbrites, Period. Mineral., 56, 285–293, 1987.

Leicher, N., Zanchetta, G., Sulpizio, R., Giaccio, B., Wagner, B., Nomade, S., Francke, A., and Del Carlo, P.: First tephrostratigraphic results of the DEEP site record from Lake Ohrid, Macedonia, Biogeosciences Discuss., 12, 15411–15460, doi:10.5194/bgd-12-15411-2015, 2015.

Lenz, O. K., Wilde, V., and Riegel, W.: Short-term fluctuations in vegetation and phytoplankton during the middle Eocene greenhouse climate; a 640-kyr record from the Messel oil shale (Germany), Int. J. Earth Sci., 1851–1874, 2011.

Lindhorst, K., Krastel, S., Reicherter, K., Stipp, M., Wagner, B., and Schwenk, T.: Sedimentary and tectonic evolution of Lake Ohrid (Macedonia/Albania), Basin Res., 27, 84–101, 2015.

Lisiecki, L. E. and Raymo, M. E.: A Pliocene-Pleistocene stack of 57 globally disturbed benthic δ^{18}O records, Paleoceanography, 20, PA1003, doi:10.1029/2004pa001071, 2005.

Lisiecki, L. E. and Raymo, M. E.: Plio-Pleistocene climate evolution; trends and transitions in glacial cycle dynamics, Quaternary Sci. Rev., 26, 56–69, 2007.

Marra, F., Karner, D. B., Freda, C., Gaeta, M., and Renne, P. R.: Large mafic eruptions at the Alban Hills volcanic district (Central Italy): chronostratigraphy, petrography and eruptive behaviour, J. Volcanol. Geoth. Res., 179, 217–232, 2009.

Milanković, M.: Théorie mathématique des phénomènes thermiques produits par la radiation solaire, Gauthier-Villars et Cie, Paris, 1920.

Molinie, A. J. and Ogg, J. G.: Milankovitch cycles in Upper Jurassic and Lower Cretaceous radiolarites of the Equatorial Pacific; spectral analysis and sedimentation rate curves, Proceedings of the Ocean Drilling Program, Scientific Results, 129, 529–547, 1990a.

Molinie, A. J. and Ogg, J. G.: Sedimentation-rate curves and discontinuities from sliding-window spectral analysis of logs, Log. Anal., 31, 370–374, 1990b.

Nomade, S., Knight, K. B., Beutel, E., Renne, P. R., Verati, C., Feraud, G., and Marzoli, A.: Duration and eruptive chronology of CAMP; implications for central Atlantic rifting and the Triassic-Jurassic boundary, Eos, Transactions, American Geophysical Union 86, @AbstractV13A-0519, 2005.

Nowaczyk, N. R., Haltia, E. M., Ulbricht, D., Wennrich, V., Sauerbrey, M. A., Rosén, P., Vogel, H., Francke, A., Meyer-Jacob, C., Andreev, A. A., and Lozhkin, A. V.: Chronology of Lake El'gygytgyn sediments – a combined magnetostratigraphic, palaeoclimatic and orbital tuning study based on multi-parameter analyses, Clim. Past, 9, 2413–2432, doi:10.5194/cp-9-2413-2013, 2013.

Pälike, H.: Earth; orbital variation (including Milankovitch cycles), Elsevier Academic Press, Oxford, United Kingdom, 410–421, 2005.

Paulissen, W. E. and Luthi, S. M.: High-frequency cyclicity in a Miocene sequence of the Vienna Basin established from high-resolution logs and robust chronostratigraphic tuning, Palaeogeogr. Palaeocl., 307, 313–323, 2011.

Petrosino, P., Jicha, B. R., Mazzeo, F. C., and Russo Ermolli, E.: A high resolution tephrochronological record of MIS 14-12 in the Southern Apennines (Acerno basin, Italy), J. Volcanol. Geoth. Res., 274, 34–50, 2014.

Priestley, M. B.: Spectral analysis and time series, Academic Press, New York, 1981.

Prokopenko, A. A., Williams, D. F., Karabanov, E. B., and Khursevich, G. K.: Continental response to Heinrich events and Bond cycles in sedimentary record of Lake Baikal, Siberia, Global Planet. Change, 28, 217–226, 2001.

Prokopenko, A. A., Hinnov, L. A., Williams, D. F., and Kuzmin, M. I.: Orbital forcing of continental climate during the Pleistocene; a complete astronomically tuned climatic record from Lake Baikal, SE Siberia, Quaternary Sci. Rev., 25, 3431–3457, 2006.

Rider, M. H. and Kennedy, M.: The Geological Interpretation of Well Logs. 3rd Edn., Rider-French Consulting Limited, Glasgow, Scotland, 2011.

Rotolo, S. G., Scaillet, S., La Felice, S., and Vita-Scaillet, G.: A revision of the structure and stratigraphy of pre-Green Tuff ingimbrites at Pantelleria (Strait of Sicily), J. Volcanol. Geoth. Res., 250, 61–74, 2013.

Scholz, C. A., Talbot, M. R., Brown, E. T., and Lyons, R. P.: Lithostratigraphy, physical properties and organic matter variability in Lake Malawi drillcore sediments over the past 145,000 years, Palaeogeogr. Palaeocl., 303, 38–50, 2011.

Serra, O. and Serra, L.: Well Logging and Geology, Serralog 2003, France, 2003.

Steiger, R. H. and Jäger, E.: Subcommission on geochronology: Convention on the use of decay constants in geo- and cosmochronology, Earth Planet. Sc. Lett., 36, 359–362, 1977.

Stockhecke, M., Kwiecien, O., Vigliotti, L., Anselmetti, F. S., Beer, J., Çağatay, M. N., Channell, J. E. T., Kipfer, R., Lachner, J., Litt, T., Pickarski, N., and Sturm, M.: Chronostratigraphy of the 600,000 year old continental record of Lake Van (Turkey), Quaternary Sci. Rev., 104, 8–17, 2014.

Sulpizio, R., Zanchetta, G., D'Orazio, M., Vogel, H., and Wagner, B.: Tephrostratigraphy and tephrochronology of lakes Ohrid and Prespa, Balkans, Biogeosciences, 7, 3273–3288, doi:10.5194/bg-7-3273-2010, 2010.

Theys, P. P.: Log data acquisition and quality control, Editions Technip, Paris, France, 1991.

Torrence, C. and Compo, G. P.: A Practical Guide to Wavelet Analysis, B. Am. Meteorol. Soc., 79, 61–78, 1998.

Trajanovski, S., Albrecht, C., Schreiber, K., Schultheiß, R., Stadler, T., Benke, M., and Wilke, T.: Testing the spatial and temporal framework of speciation in an ancient lake species flock: the leech genus Dina (Hirudinea: Erpobdellidae) in Lake Ohrid, Biogeosciences, 7, 3387–3402, doi:10.5194/bg-7-3387-2010, 2010.

Vogel, H., Wagner, B., Zanchetta, G., Sulpizio, R., and Rosen, P.: A paleoclimate record with tephrochronological age control for the last glacial-interglacial cycle from Lake Ohrid, Albania and Macedonia, J. Paleolimnol., 44, 295–310, 2010a.

Vogel, H., Wessels, M., Albrecht, C., Stich, H.-B., and Wagner, B.: Spatial variability of recent sedimentation in Lake Ohrid (Albania/Macedonia), Biogeosciences, 7, 3333–3342, doi:10.5194/bg-7-3333-2010, 2010b.

Vogel, H., Zanchetta, G., Sulpizio, R., Wagner, B., and Nowaczyk, N.: A tephrostratigraphic record for the last glacial-interglacial cycle from Lake Ohrid, Albania and Macedonia, J. Quaternary Sci., 25, 320–338, 2010c.

Wagner, B., Reicherter, K., Daut, G., Wessels, M., Matzinger, A., Schwalb, A., Spirkovski, Z., and Sanxhaku, M.: The potential of Lake Ohrid for long-term palaeoenvironmental reconstructions, Palaeogeog. Palaeocl., 259, 341–356, 2008.

Wagner, B., Wilke, T., Grazhdani, A., Kostoski, G., Krastel, S., Reicherter, K. R., and Zanchetta, G.: SCOPSCO; Scientific Collaboration On Past Speciation Conditions in Lake Ohrid. Eos, Transactions, American Geophysical Union 90, @AbstractPP14A-02, 2009.

Wagner, B., Wilke, T., Krastel, S., Zanchetta, G., Sulpizio, R., Reicherter, K., Leng, M., Grazhdani, A., Trajanovski, S., Levkov, Z., Reed, J., and Wonik, T.: More Than One Million Years of History in Lake Ohrid Cores, EOS, Transactions, American Geophysical Union 95, 25–32, 2014.

Weedon, G.: Time-series analysis and cyclostratigraphy; examining stratigraphic records of environmental cycles, Cambridge University Press, Cambridge, United Kingdom, 2003.

Wonik, T.: Gamma-ray measurements in the Kirchrode I and II boreholes, Palaeogeogr. Palaeocl., 174, 97–105, 2001.

Wu, H., Zhang, S., Feng, Q., Jiang, G., Li, H., and Yang, T.: Milankovitch and sub-Milankovitch cycles of the early Triassic Daye Formation, South China and their geochronological and paleoclimatic implications, Gondwana Res., 22, 748–759, 2012.